Hindawi
Journal of Nanomaterials
Volume 2023, Article ID 9882964, 15 pages
https://doi.org/10.1155/2023/9882964

Research Article

Tailoring of Ag_3PO_4-Anchored Hydroxyapatite Nanophotocatalyst with Tunable Particle Size by a Facile Ion-Exchange Method for Organic Textile Dyes Photodegradation

Surendran Dhatchayani,[1] **Krishnasamy Sankaranarayanan**,[1] **and K. Kathiresan**[2]

[1]*Functional Materials Laboratory, Department of Physics, Alagappa University, Karaikudi 630003, Tamil Nadu, India*
[2]*School of Civil Engineering and Architecture, Adama Science and Technology University, Adama, Ethiopia*

Correspondence should be addressed to Krishnasamy Sankaranarayanan; hhrsankar@yahoo.com and K. Kathiresan; kathiresan.karuppanan@astu.edu.et

Received 5 August 2022; Revised 26 September 2022; Accepted 6 October 2022; Published 10 April 2023

Academic Editor: Balasubramani Ravindran

Silver phosphate (Ag_3PO_4) exhibits excellent photocatalytic performance but has limitation in its stability and reusability. To overcome the issue of reusability, composites of silver phosphate nanostructures are tailored. This paper elucidates the photocatalytic study of silver phosphate-anchored hydroxyapatite (HA) ($Ca_{10}(PO_4)_6(OH)_2$) on the degradation of commercial textile dye, Sunfix Red (SR) S3B 150% by changing the experimental parameters such as catalyst concentration, dye concentration, and pH of the dye solution under the sunlight. Silver phosphate-anchored HA (HA_$Ag_3PO_4(x)$) was prepared via a two-step process. HA was synthesized by a simple wet chemical precipitation and silver phosphate-anchored HA (HA_$Ag_3PO_4(x)$) via *in situ* ion-exchange method. The synthesized photocatalysts were subjected to characterization studies such as X-ray diffraction (XRD), Fourier transform infrared (FTIR) spectroscopy, transmission electron microscopy (TEM), ultraviolet–visible spectroscopy, and X-ray photoelectron spectroscopy (XPS). All the synthesized composites exhibited the bandgap of 2.34 eV and degraded SR in 45 min with the rate constant 0.07168 min^{-1} under sunlight. The trapping tests for radicals were done to study the role of free radicals in the degradation of the dye, SR, and the possible degradation mechanism was proposed. The postphotocatalytic analysis of XRD showed that the structure of Ag_3PO_4 remained intact declaring its structural stability. It was observed that the concentration of $AgNO_3$ precursor influenced the number of nucleation over the surface of HA and the particle size of Ag_3PO_4. The applicability of the synthesized material was extended to other organic dyes such as Sunzol Black (SB) DN conc., methylene blue (MB), and rhodamine B (RhB) by the prepared composite and the findings were presented.

1. Introduction

Exploitation of all kinds of natural resources and their replenishment is the major considerations in this age. Among these issues, water pollution and scarcity are making the situation hectic since water is an essential element of social and economic development. Therefore, many efforts have been devoted in order to conserve and sustain water resources. Urbanization and industrialization are not only exploiting the water resources, but also releasing effluents into water to such an extent that it is creating a great threat to the flora and fauna as well as humankind. The water contaminants include a wide range of chemicals, pathogens, and physical factors such as temperature, etc. [1, 2]. Textile industry is an important water-contaminant source as it consumes huge quantity of water and releases massive effluents. For the past decades, the researchers are paying much attention to the removal of textile organic pollutants by various methods which include biodegradation, electrocoagulation, photodegradation, oxidation, adsorption, and ultrafiltration [3–8]. Among them, photocatalysis has proved to be an excellent method to decompose the organic effluents being highly efficient and cost-effective [9, 10]. Due to photocatalytic efficiency and cost-effectiveness, TiO_2-based photocatalysts have been of research interest yet their practical application is limited because of their higher bandgap energy which

falls in the UV region [10]. Many researchers focus on other intriguing materials such as g-C_3N_4-, SnO_2-, and ZnO-based heterostructured photocatalysts owing to their tunable bandgaps and photocatalytic efficiency [6, 8, 11].

For recent years, Ag_3PO_4 is being an intriguing candidate for photocatalytic degradation. Ag_3PO_4 possesses high photocatalytic efficiency and its quantum efficiency is nearly 90% [12]. In addition to that, the bandgap of Ag_3PO_4 is 2.34 eV, which makes it suitable for solar-light-driven photocatalysis. In this regard, Ag_3PO_4 can be undoubtedly an interesting candidate to be studied. Nevertheless, its higher solubility and poor stability hinder its vast application [9]. Ag_3PO_4 is vulnerable to photocorrosion. However, Ag_3PO_4-based heterogeneous composites have been gaining substantial attention due to their enhanced physical and chemical properties, which make them outstanding photocatalysts [13, 14]. Hydroxyapatite (HA) is the inorganic mineral phase of biological hard tissues and is abundant in nature. HA is a remarkable candidate in biomedical as well as environmental applications due to its exceptional biocompatibility, nontoxicity, structural flexibility, facile synthesis, and cost-effectiveness [15, 16]. HA is being tailored with tunable characteristics in a variety of applications owing to (1) the flexibility of the apatite structure that enables HA to host almost half of the elements in the periodic table, (2) an effortless ion-exchange process facilitates the replacement of Ca^{2+} ions in HA by a wide range of ions, and (3) substitution of both anions and cations is possible, i.e., PO_4^{3-} and OH^- functionalities in the apatite structure can be easily replaced by a variety of species like SeO_3^{2-}, VO_4^{3-}, SiO_4^{2-}, CO_3^{2}, and halides [17–19]. Moreover, HA can be a prominent substrate for a photocatalyst like Ag_3PO_4 for the following features: (1) adsorption capability of the catalyst is very crucial in photocatalysis process and HA can serve this being a well-known adsorbent for inorganic and organic matters, (2) mass transfer limitations can be reduced, (3) hinders the photogenerated electron–hole recombination by effective separation, (4) heterostructures can easily be tailored, and (5) possesses excellent thermal stability, biodegradability, and nontoxicity [9, 15, 20].

In this work, HA_Ag_3PO_4 composites were synthesized in two steps in which neat hydroxyapatite was synthesized via chemical precipitation technique and Ag_3PO_4 nanoparticles were anchored on hydroxyapatite via a facile and at the same time very effective postsynthesis process, ion-exchange method [21]. Still, more studies are required in order to explore the behaviors of the photocatalyst for different dyes. In this work, the photocatalytic behavior of Ag_3PO_4 composite in the degradation of the commercial textile dye Sunfix Red (SR) S3B 150% for the first time was studied, and also the degradation under different experimental conditions was investigated. Moreover, the applicability of the prepared composites on other commercial dyes was examined.

2. Experimental

2.1. Materials. All the reagents of analytical grade were purchased and used without further purification. Calcium nitrate tetrahydrate ($Ca(NO_3)_2{\cdot}4H_2O$), diammonium hydrogen phosphate ($(NH_4)_2HPO_4$), silver nitrate ($AgNO_3$), and NH_4OH 25% were obtained from Merck, Germany.

2.2. Preparation of Neat HA. The neat HA was prepared by wet chemical precipitation technique reported elsewhere [22] which initially involves the preparation of 0.5 M calcium nitrate solution and 0.3 M diammonium hydrogen phosphate solution. Then, the phosphate solution was added to the calcium precursor at temperature 60°C. The pH of the reaction solution was maintained at 10.5 by adding sufficient amount of ammonium hydroxide and was stirred for 2 hr at 60°C followed by 24 hr aging. Later, the precipitate was filtered and washed many times with deionized water and ethanol. Subsequently, the precipitate was dried at 70°C for 24 hr. The chemical reaction is given as follows:

$$10Ca(NO_3)_2 + 2H_2O + 6(NH_4)_2HPO_4 + 8NH_3 \longrightarrow Ca_{10}(PO_4)_6(OH)_2 + 20NH_4NO_3. \quad (1)$$

2.3. Preparation of Ag_3PO_4-Anchored HA (HA_Ag_3PO_4(x)). Ag_3PO_4-anchored HA was synthesized via *in situ* ion-exchange process reported elsewhere [14] and the schematic illustration is given in Figure 1. A hundred milliliters of $AgNO_3$ solution of appropriate concentration (0.02, 0.05, 0.08 M) was added dropwise into the aqueous dispersion of HA (3 g in 100 mL of deionized water). Subsequently, it was subjected to a vigorous and continuous stirring for 4 hr under dark condition. Then, the composite was separated by centrifugation, washed repeatedly with distilled water, and dried at 60°C in vacuum oven overnight. By this way, the nanocomposites were prepared with different $AgNO_3$ concentrations of 0.02, 0.05, and 0.08 M and named as HA_Ag_3PO_4(a), HA_Ag_3PO_4(b), and HA_Ag_3PO_4(c), respectively.

2.4. Characterization Techniques. The structural characterization was carried out through X-ray diffraction (XRD) pattern of the sample, which was recorded by a PANalytical X'Pert Pro X-ray diffractometer ($\lambda = 1.5418$ Å) at room temperature. The functional groups of the prepared samples were identified using Fourier transform infrared (FTIR) spectrometer (Perkin Elmer-Spectrum RX I). X-ray photoelectron spectra (XPS) was recorded by a PHI VersaProbe III photoelectron spectrometer and the surface chemical composition and valence state of the prepared samples were studied. The morphologies of samples were examined by JEOL-2100+ high-resolution transmission electron microscope. The optical properties of the samples were analyzed using the UV–vis spectrometer (Thermo Fisher Evolution 220). The concentration of the dye solutions was studied by Electra photometer.

2.5. Analysis of Photocatalytic Performance of the Prepared Composites. The photocatalytic behavior of the prepared samples was investigated through the photodegradation of the commercial organic dyes under sunlight. Initially, the anionic organic dye SR S3B 150% ($C_{44}C_{l2}H_{24}N_{14}Na_6O_{20}S_6$) was taken as a model and the photodegradation was evaluated under different experimental conditions such as Ag_3PO_4 concentration, dosage of photocatalyst, and concentration of

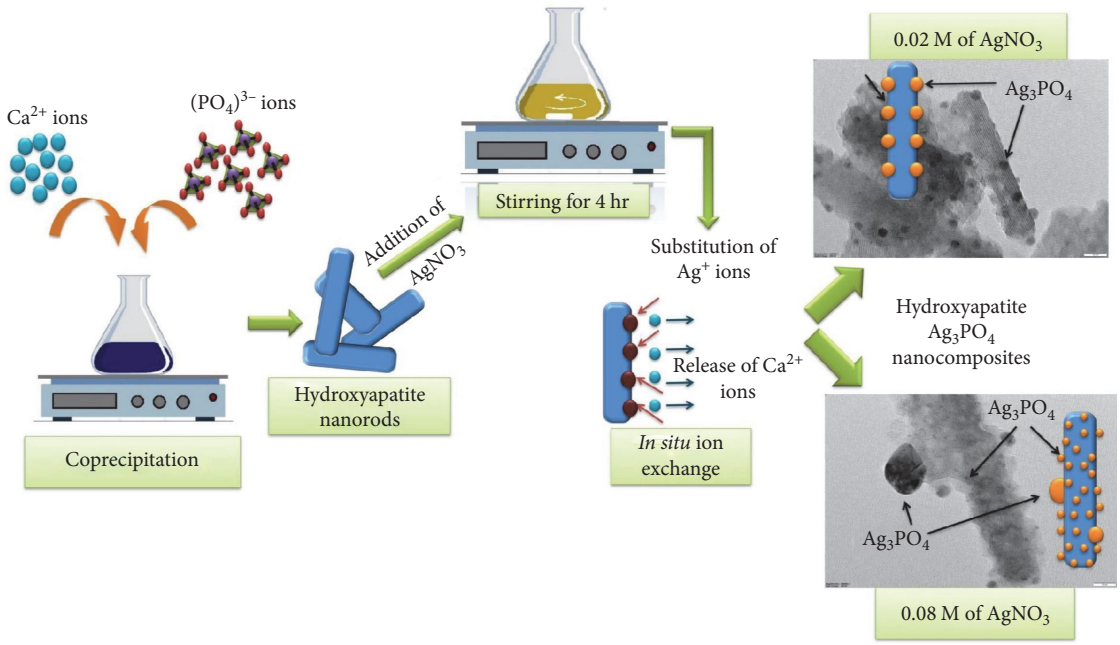

Figure 1: Schematic illustration of the experiment for preparing Ag_3PO_4-anchored HA.

the dye solution. In addition to these, the initial pH of the solution also influences the adsorption and degradation process and, hence, it is very essential for consideration [23]. Therefore, the photodegradation of the dye solution with different initial pH values was also examined. Later, the photocatalytic activity of the selected photocatalyst was also extended to other organic dyes, namely, Sunzol Black (SB) DN conc. (anionic), methylene blue (MB; cationic), rhodamine B (RhB; cationic), and cocktail (CT) of the aforementioned four different dyes. The required concentration of dye solutions was prepared and the initial pH of the dye solutions were adjusted with 2 mol/l NaOH solution or concentrated HNO_3. The appropriate amounts of catalysts were added to the dye solutions and were magnetically stirred for 1 hr in dark condition to attain adsorption and desorption equilibrium before photocatalytic studies. After irradiation with sunlight, the aliquots were collected in equal intervals and the concentration of the centrifuged aliquots was determined using UV–visible spectrometer. The decolorization rate of the dyes ($D\%$) were calculated by the following equation:

$$D\% = \frac{(C_0 - C)}{C_0} \times 100, \quad (2)$$

where C_0 and C were the initial and instantaneous concentrations of the dye solution, respectively.

The role of active radical species in the photocatalytic degradation process was also examined by applying scavengers. The scavengers such as isopropyl alcohol (IPA), disodium ethylenediaminetetraacetate (EDTA), and ascorbic acid were used to trap the hydroxyl (·OH), photogenerated holes (h^+), and superoxide ($\cdot O_2^-$) radicals, respectively. The scavengers were added to the organic dye solutions at a concentration of 1 mmol/L before the addition of photocatalyst and subjected to the photocatalytic degradation as abovementioned.

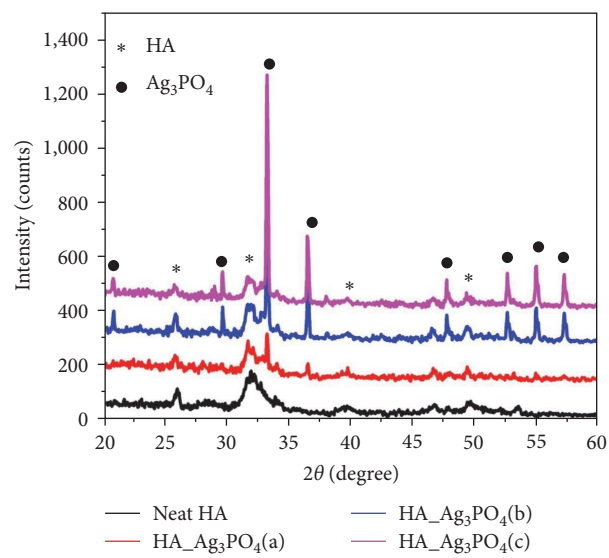

Figure 2: XRD patterns of neat HA and the nanocomposites.

3. Results and Discussion

3.1. Characterization of the Prepared Composites

3.1.1. XRD Analysis. The XRD patterns of as-prepared neat HA and HA_Ag_3PO_4(x) composites were presented in Figure 2. The XRD patterns of all the samples were indexed against HA (JCPDS# 009-0432) and Ag_3PO_4 (JCPDS Card#006-0505). The XRD patterns of HA_Ag_3PO_4(x), as shown in Figure 2,

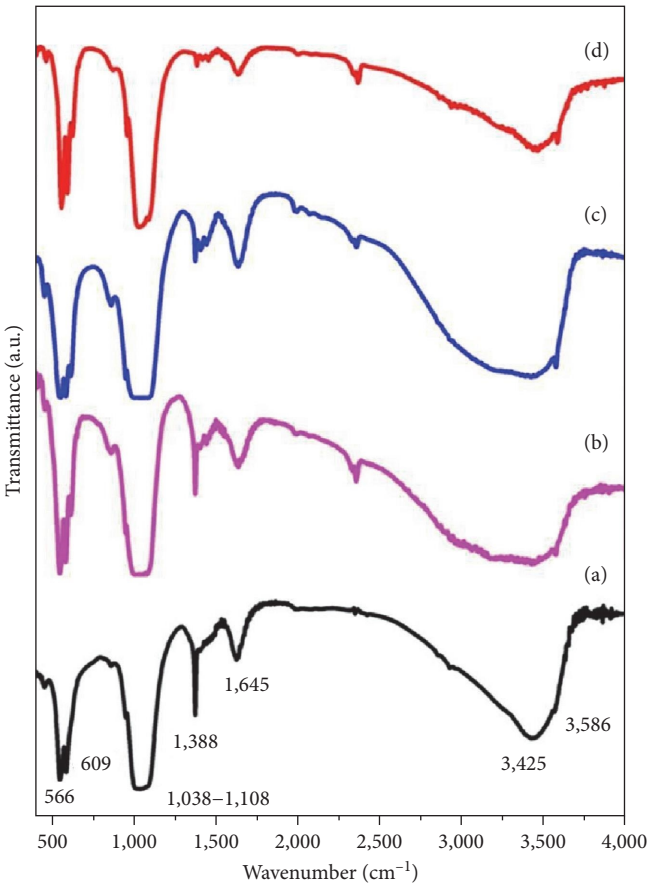

FIGURE 3: FTIR spectra of neat HA (a); HA_Ag_3PO_4(a) (b); HA_Ag_3PO_4(b) (c); HA_Ag_3PO_4(c) (d).

evidence the presence of Ag_3PO_4 in the background of HA. Besides, the intensities of the peaks representing Ag_3PO_4 get increased with the increase in $AgNO_3$ molar ratio; meanwhile, the characteristic HA peaks remain intact suggesting that the ion-exchange process proceeded by retaining the structure of HA. Further, it ascertains the composite nature of the HA_Ag_3PO_4(x).

3.1.2. FTIR Analysis. FTIR spectra of the prepared samples are depicted in Figure 3 and are exhibiting the signature bands of hydroxyapatite. The bending vibrational modes of PO_4^{3-} are identified at 566 and 610 cm^{-1} and the absorption bands corresponding to 1,038–1,108 and 967 cm^{-1} are ascribed to the stretching vibration modes of PO_4^{3-}. The presence of absorption peaks at 1,389 and 1,645 cm^{-1} approves the incorporation of carbonate ions in HA structure. The presence of hydroxyl group is confirmed by the absorption at 3,586 cm^{-1} and the broad band around 3,425 cm^{-1} is due to the absorbed water [24, 25]. The absorption regions (967 and 1,080 cm^{-1}) of asymmetric stretching of P–O–P associated with Ag_3PO_4 coincide with the signature phosphate bands of HA and no metal Ag-related bands in the observed FTIR spectra of the composites (b–d), as shown in Figure 3, were detected [26].

3.1.3. XPS Analysis. Neat HA and HA_Ag_3PO_4(c) were subjected to the XPS analysis and Figures 4 and 5 display their corresponding spectra. The wide range spectra of neat and composite HA exhibit the presence of the elements of hydroxyapatite and additionally Ag in the composite. The characteristic doublet at the binding energies 373.35 and 367.46 eV corresponding to Ag^+ was evidenced for the sample HA_Ag_3PO_4(c) (Figure 5(d)), which strongly suggests the presence of Ag_3PO_4 in the composite [27, 28]. While examining the core level spectra of Ca and P in the samples HA and HA_Ag_3PO_4(c), there is no significant shift found as the corresponding binding energies to Ca $2p_{3/2}$ and Ca $2p_{1/2}$ were detected around 346.5 and 350 eV, and for P, it was observed around 132.5 eV [29]. The deconvolution of O 1s core spectra of HA_Ag_3PO_4(c) discloses three distinct peaks. The binding energy 529.5 eV is ascribed to the lattice oxygen of Ag_3PO_4, which is absent in that of neat HA. The other two peaks are of binding energies 530.9 and 532.6 eV. The earlier is assigned to the oxygen atoms in P=O and the later can be contributed by the oxygen from O–H [29].

In addition, the photoelectron peaks corresponding to C 1s were also identified. It is quite common to get carbonated hydroxyapatite since the synthesis method in open air facilitates the incorporation of atmospheric carbonates in the HA structure. The photoelectron peaks around 284.5 and 286.1 eV are representing to C–C and C–O–C of the absorbed hydrocarbons, whereas 288.2 eV is ascribed to C=O bonds in carbonate [30].

3.1.4. TEM Analysis. The morphological features of the synthesized neat HA and HA-anchored Ag_3PO_4 composites are depicted in Figure 6. The neat HA prepared via simple wet precipitation method exhibited nanorod morphology (Figure 6(a)). While examining the TEM image of composite HA_Ag_3PO_4(a), the homogeneous distribution of Ag_3PO_4 spheres of size about 4 nm over the surface of hydroxyapatite is evidenced (Figure 6(d)). The TEM investigation was also extended to the composite HA_Ag_3PO_4(c) with the highest Ag^+ concentration in the present study, which is presented in Figures 6(e) and 6(f). Interestingly, Ag_3PO_4 formations are found to be greater in number than that could be observed in the case of HA_Ag_3PO_4(a) (lower Ag^+ concentration). The higher Ag^+ concentration (0.08 M) facilitated a larger amount of nucleations over HA surface and also resulted in the reduction of Ag_3PO_4 particle size as indicated by blue arrows in Figure 6(e). Due to the decline in particle size, the surface area to volume ratio was expected to increase, which is a more favorable condition for photocatalysis [27]. Meanwhile, few larger sized Ag_3PO_4 spheres around 5 and 15 nm were also observed on HA as indicated by yellow arrows in Figure 6(e).

3.1.5. UV–Vis Diffuse Reflectance Spectroscopy. The UV–visible diffuse reflectance spectra (DRS) of pure HA and HA_Ag_3PO_4(x) are shown in Figure 7 and their bandgaps are depicted in Figure 8. Investigation of the bandgaps (Figure 8) gives the essential information about the photocatalytic behavior under visible light. The bandgap of neat HA was found to be 3.4 eV, whereas the composites (HA_Ag_3PO_4(x)) exhibited bandgap energy of 2.34 eV. The narrowed bandgap (2.34 eV) of the composites is due to the

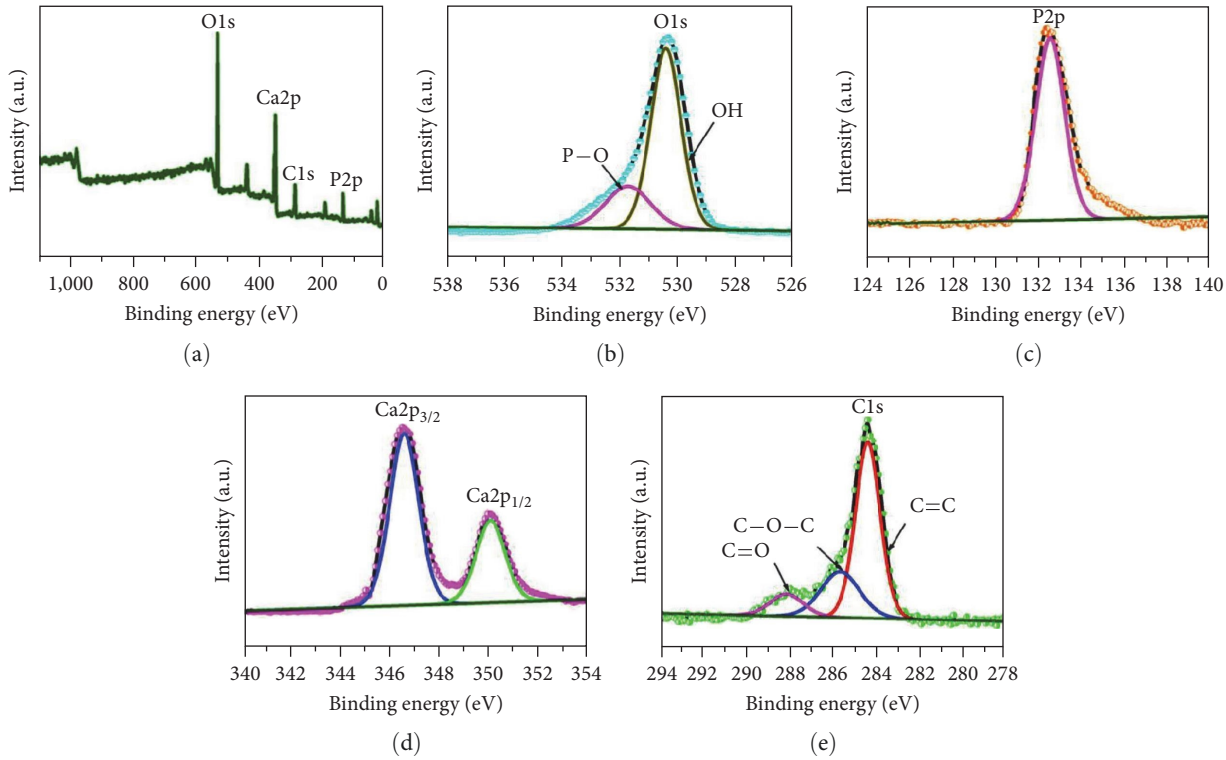

FIGURE 4: XPS spectra of neat HA.

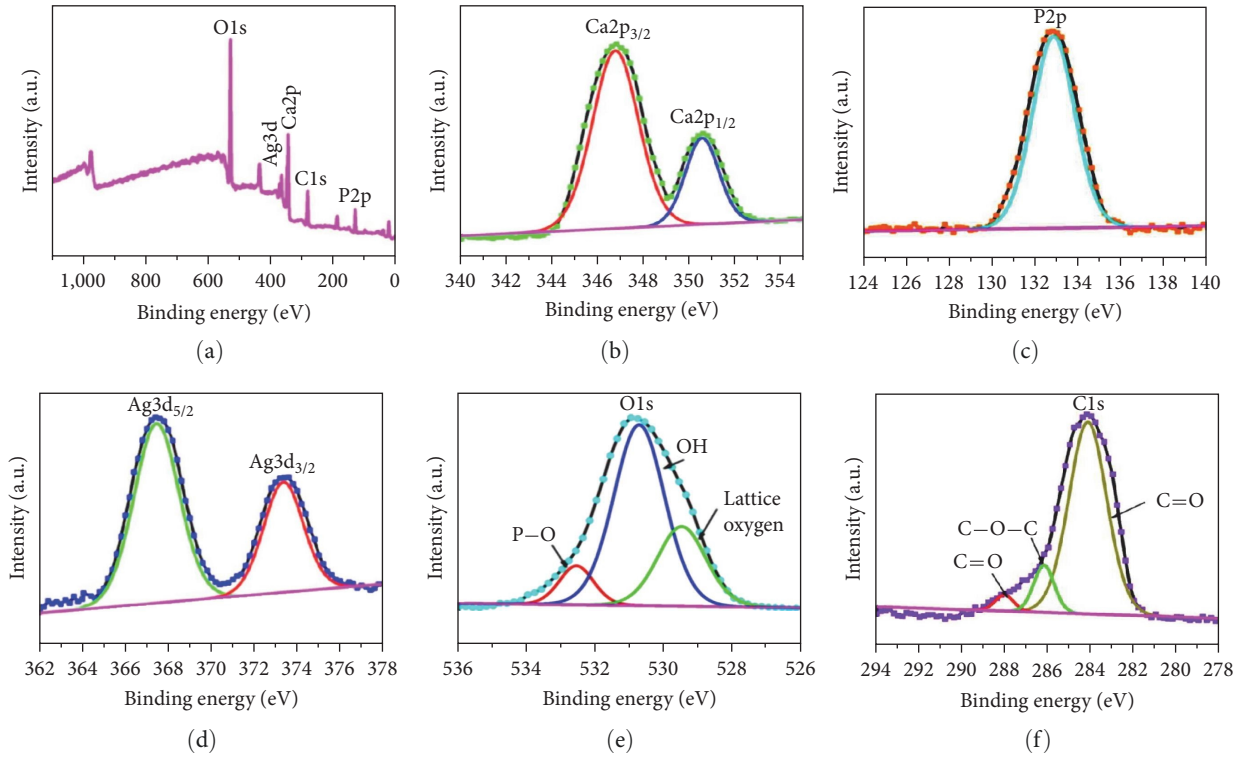

FIGURE 5: XPS spectra of HA_Ag_3PO_4(c).

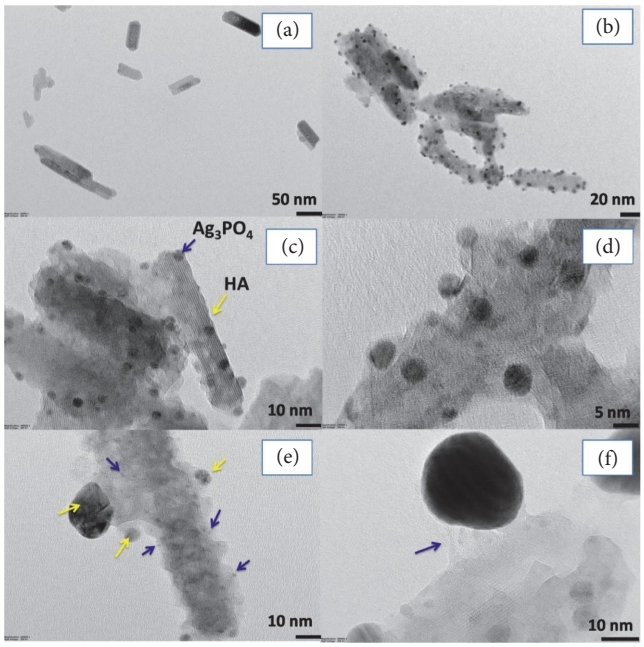

Figure 6: TEM images of neat HA (a); HA_Ag_3PO_4(a) at different magnifications (b–d); HA_Ag_3PO_4(c) at different magnifications (e and f).

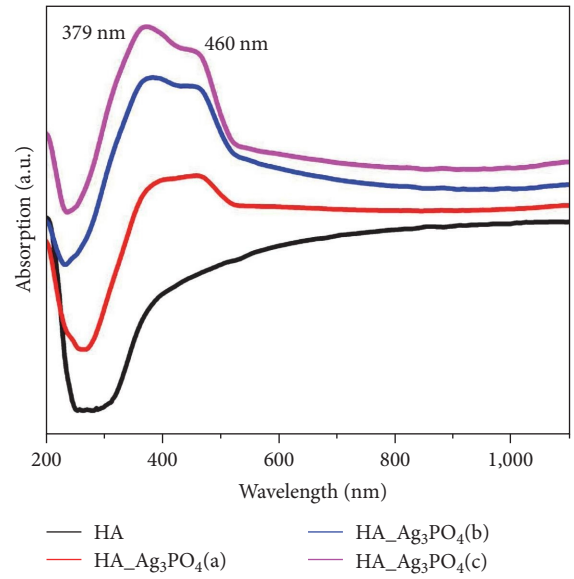

Figure 7: UV–visible diffuse reflectance spectra of neat HA and the composites.

presence of Ag_3PO_4 which is well matched with the reported values of Ag_3PO_4 [28] and enables the photocatalyst to perform under visible light.

In addition to the bandgap, the valence band and conduction band edge potentials were also estimated by the following empirical formula:

$$E_{VB} = \chi - E^c + 0.5E_g, \tag{3}$$

$$E_{CB} = E_{VB} - E_g, \tag{4}$$

where E_{VB} and E_{CB} are the valence band and conduction band edge potentials, respectively; χ is Mulliken electronegativity of Ag_3PO_4 which is the geometric mean of the electronegativity of the constituent atoms and it was calculated to be 5.96 eV; E^c represents the energy of free electrons on the hydrogen scale (−4.5 eV); and E_g is the bandgap energy of Ag_3PO_4. Thus, calculated VB and CB potentials of Ag_3PO_4 are 2.63 and 0.29 eV, respectively.

3.2. Photocatalytic Degradation of Organic Dyes. The photocatalytic degradation of all the selected organic dyes in the presence of the prepared photocatalysts were analyzed after 60 min adsorption and considered as 0 min for photocatalysis process in sunlight. First, photodegradation of the anionic dye SR S3B 150% was carried out under different conditions such as dye concentration, photocatalyst concentration, and pH of the dye solution, and their influence on the degradation of the dye was investigated. In addition, blank dye solution in the absence of photocatalyst was also examined as a control. For the better investigation of the photocatalytic behavior of the prepared samples, zero-order, first-order, and second-order kinetic studies were carried out and the rate constants were determined by the following equations:

zero-order kinetic equation:

$$C_0 - C = k_0 t, \tag{5}$$

first-order kinetic equation:

$$\ln\left(\frac{C_0}{C}\right) = k_1 t, \tag{6}$$

second-order kinetic equation:

$$\frac{1}{C} - \frac{1}{C_0} = k_2 t, \tag{7}$$

where k_0, k_1, and k_2 are the rate constants of zero-, first-, and second-order kinetics, respectively; C_0 and C are the concentrations of the dye solution before and after irradiation at time, t.

3.2.1. Effect of Ag_3PO_4 Loading on HA. The adsorption under dark condition and photodegradation of the model dye pollutant SR S3B 150% (20 ppm) under visible light (sunlight) at a fixed dosage concentration of 0.5 g L^{-1} were studied and presented in Figure 9. It is evidenced that the adsorption capacity of the photocatalyst is increased with Ag_3PO_4 concentration. The blank dye solution and with HA did not show a significant degradation under sunlight irradiation, whereas the composites HA_Ag_3PO_4(x) exhibited photocatalytic activity with an increasing trend with increase in Ag_3PO_4 concentration with rate constants 0.00515, 0.02178, and 0.07168 min^{-1}, respectively (Table 1). The composite HA_Ag_3PO_4(c) has the highest rate constant compared with other photocatalysts used in this study and, hence, HA_Ag_3PO_4(c) was selected for further photodegradation investigations. The highest performance of HA_Ag_3PO_4(c)

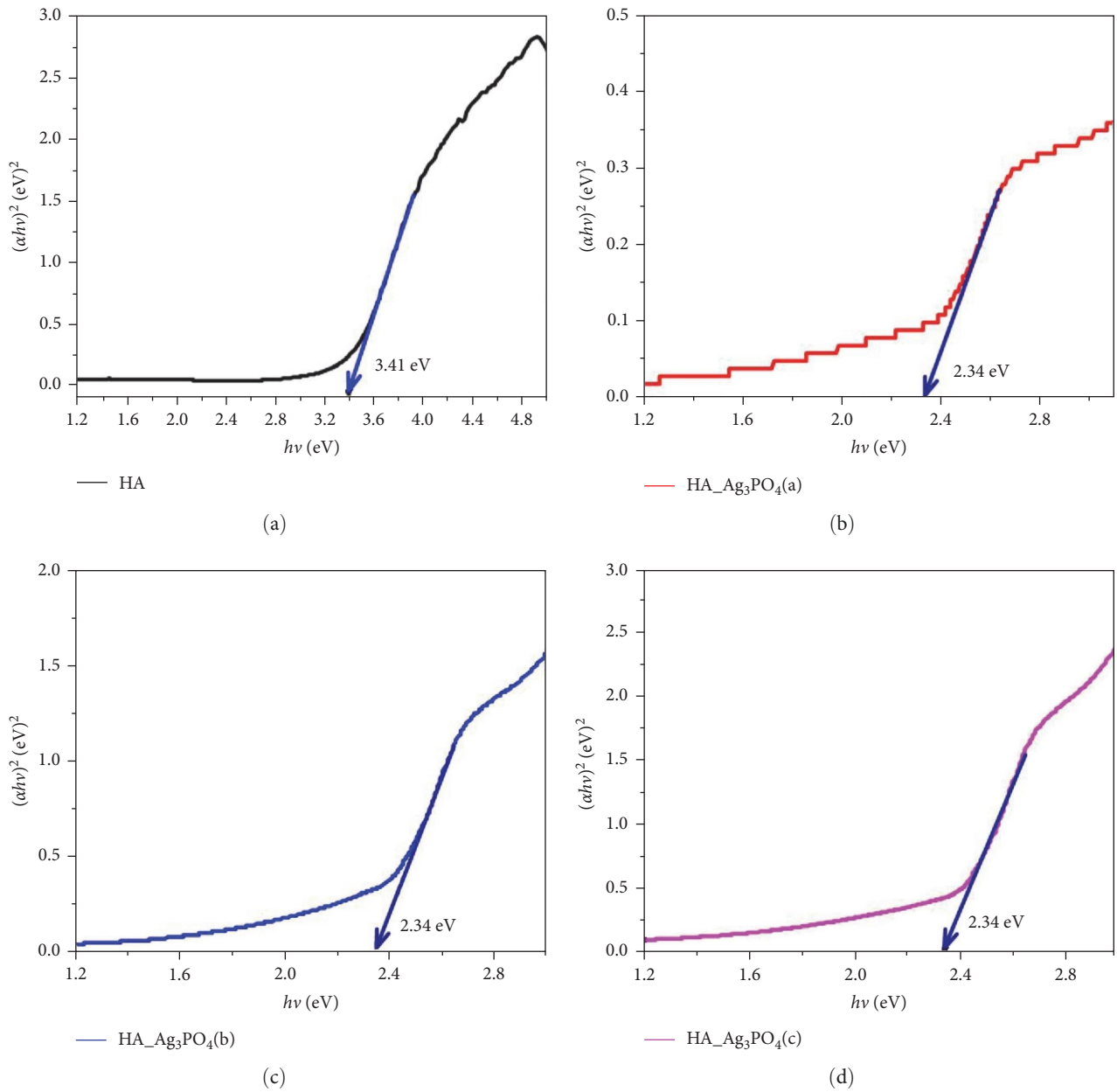

Figure 8: Bandgaps of neat HA (a) and prepared composites (c–d).

can be explicitly understood that the higher amount of Ag_3PO_4 gives rise to higher active sites, which leads to higher production of reactive radical species. This is also confirmed by TEM image of HA_Ag_3PO_4(c) (Figure 6(e)), which revealed the larger number of Ag_3PO_4 particles on HA and also it is in agreement with XRD result. Moreover, it is very clear from TEM result that the Ag_3PO_4 particles formed by ion substitution on HA substrate have a declined particle size compared with the lower Ag^+ concentration, which in turn enhances the active surface area of the material. The surface area of the photocatalytic material is one of the very important parameters to influence photocatalysis [27].

3.2.2. Effect of Dosage of HA_Ag_3PO_4(c). From the above findings, it is evident that the composite HA_Ag_3PO_4(c) performed an excellent photocatalytic activity and, hence, HA_Ag_3PO_4(c) was taken for further studies. The dependence of HA_Ag_3PO_4(c) on dosage concentration in the photocatalytic degradation of SR S3B 150% was examined. The photocatalyst concentration range was selected from 0.25 to 2 g L^{-1} at the dye concentration of 20 ppm and their photocatalytic performances were examined for 1 hr, as depicted in Figure 10. As the photocatalyst quantity increased, an increasing trend of degradation of the dyes can be noticed. It is general to have an increasing photodegradation as the number of active sites on the surfaces of the photocatalyst increases. Consequently, it gives rise to large number of reactive radical species. At the end of the photocatalysis (60 min irradiation), the lowest concentration of HA_Ag_3PO_4(c) (0.25 g L^{-1}) degraded the dye to 53%, while the other

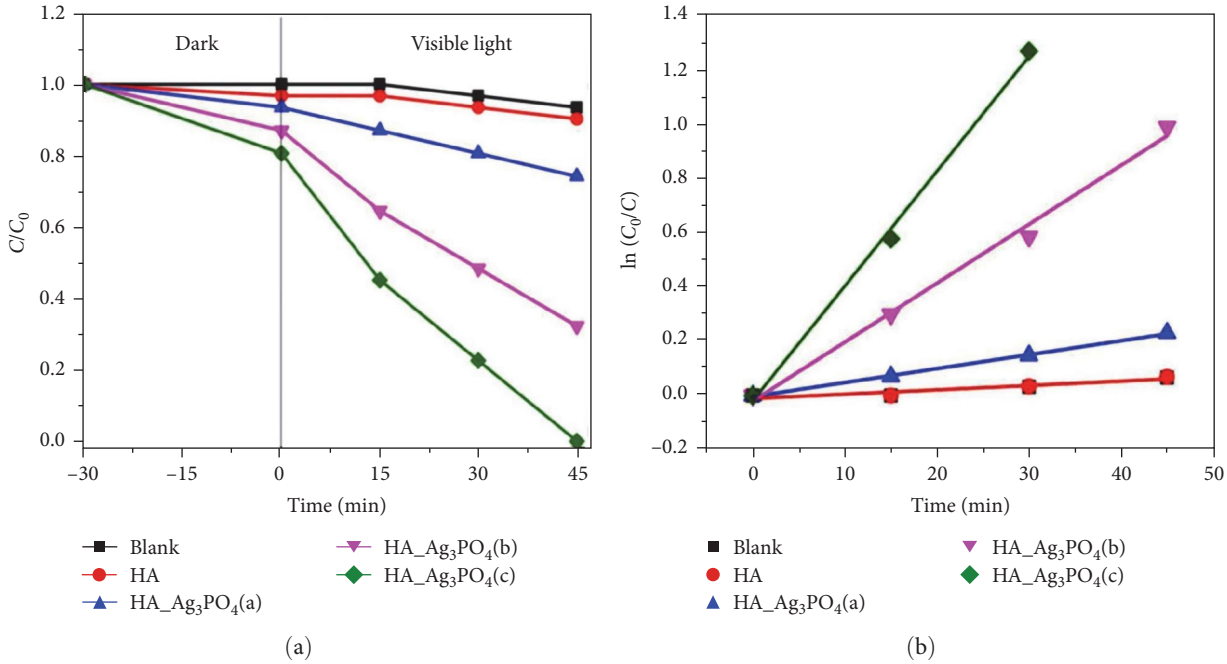

Figure 9: Effect of Ag_3PO_4 loading: photocatalytic performance of neat HA and Ag_3PO_4 composites on SR under visible light.

Table 1: Kinetics studies of the photocatalytic degradation of SR by the prepared photocatalysts.

Catalysts	Catalyst concentration ($g\,L^{-1}$)	Zero order $C_0 - C = k_0 t$		First order $\ln(C_0/C) = k_1 t$		Second order $(1/C) - (1/C_0) = k_2 t$	
		k_0 (min^{-1})	R^2	k_1 (min^{-1})	R^2	k_2 (min^{-1})	R^2
HA_Ag_3PO_4(a)	0.5	0.00133	0.99782	0.00515	0.99821	0.03895	0.58407
HA_Ag_3PO_4(b)	0.5	0.00373	0.98861	0.02178	0.98989	0.0294	0.944
HA_Ag_3PO_4(c)	0.5	0.0055	0.89646	0.07168	0.98209	0.16905	0.92962

concentrations 0.5, 1 and 1.5 $g\,L^{-1}$ degraded the dye completely at 45, 30, and 15 min, respectively. The rate constants obtained from ln (C_0/C) versus time plot for the concentrations 0.25, 0.5, 1, and 1.5 are 0.009, 0.034, 0.046, and 0.0924, respectively. In the same time, the dye was completely adsorbed at the maximum concentration of 2 $g\,L^{-1}$ and the sample dye solution became turbid. Hence, the concentration of HA_Ag_3PO_4(c) is limited to 1.5 $g\,L^{-1}$.

3.2.3. Effect of Initial Concentration of the Dye Solution. The impact of initial concentration of the dye solution on photodegradation of SR S3B 150% was studied in the range from 10 to 50 ppm at a fixed photocatalyst concentration 0.5 $g\,L^{-1}$, which is presented in Figure 11. It was observed that the percentage of degradation was declined with the increase in dye concentration. The dye solution of concentrations 10 ppm at 30 min were undergone degradation of 100% while the rest of the concentrations 20–50 ppm showed a degradation of 66.6%, 53.8%, 47.2%, and 44%, respectively, at 30 min. A declining trend in the rate constants for the degradation process of increasing concentration was noticed (10, 20, 30, 40, and 50 ppm—0.04621, 0.03662, 0.02613, 0.02246, and 0.01921 min^{-1}, respectively). This can be clarified by two ways as follows: one reason can be the limitation of the number of active sites on the photocatalyst surface which may be insufficient to degrade the higher concentrations and the other can be explained in terms of amount of adsorption of dyes. As the increase in dye concentration leads to higher amount of dye to be adsorbed on the catalyst surface, it shields the catalyst from the radiation and hinders the photogeneration of the electron–hole pair which is responsible for the degradation of the dye [23, 31, 32].

3.2.4. Effect of Initial pH of the Dye Solution. The initial pH of the polluted solution is a crucial influencing factor in controlling the photodegradation process. The pH affects the surface charge of the catalyst, pollutants adsorption onto the catalyst, and the valence band oxidation potential [33, 34]. The photocatalytic behavior of the selected photocatalyst, in the degradation of SR S3B 150% under a broad range of pH conditions from 2 to 10 with two-step variation, was examined at a fixed irradiation time of 15 min. The results revealed that acidic condition favored the enhanced photodegradation than neutral condition. The maximum photodegradation of the organic dye SR was observed to be 96.8% at pH 4 and also at pH 2 and 6 comparable degradation efficiency (93.5% for

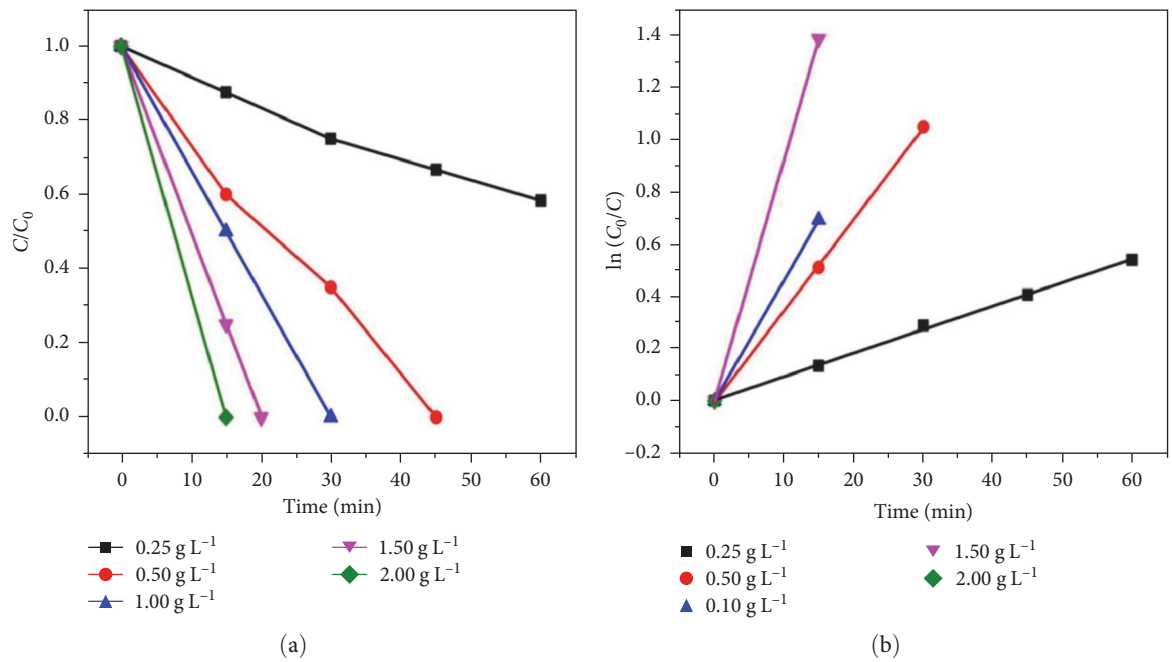

Figure 10: Photocatalytic performance of HA_Ag_3PO_4(c) of different dosage concentrations on SR under visible light.

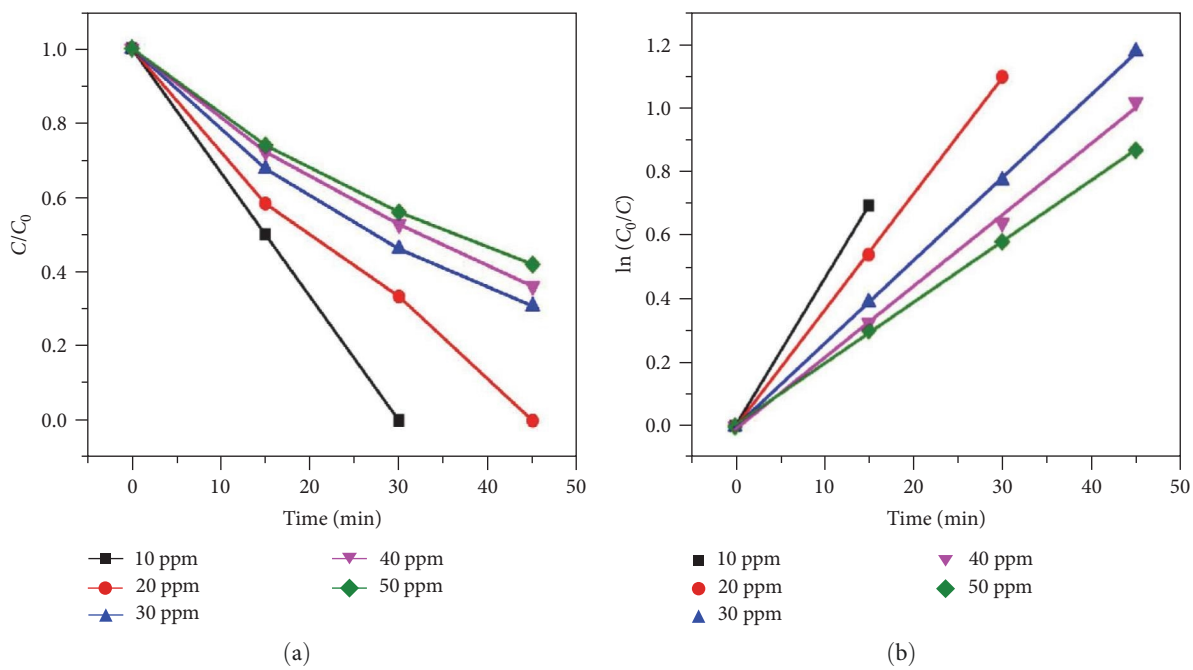

Figure 11: Effect of dye concentration on photocatalytic degradation of SR under visible light.

both) were noticed, but very low degradation efficiencies were found at higher pH values. As shown in Figure 12(a), it is evidenced that the higher adsorption facilitated higher photodegradation. At acidic conditions, Ag_3PO_4 becomes positively charged and the higher adsorption of the anionic dye SR occurred due to the electrostatic attraction between the pollutant and catalyst. In the same time, at basic conditions, the deprotonated OH^- groups over the catalyst surface hinder the adsorption of the anionic dye by electrostatic repulsion [35]. Even though the higher pH resulted in lower adsorption, a faster degradation was observed at pH 10. This could be due to the lowering of the oxidation potential of the dye and eventually the dye can be degraded quickly [36].

3.2.5. Quenching Test. The free radicals employed in the photocatalytic process, namely, such as hydroxyl (·OH),

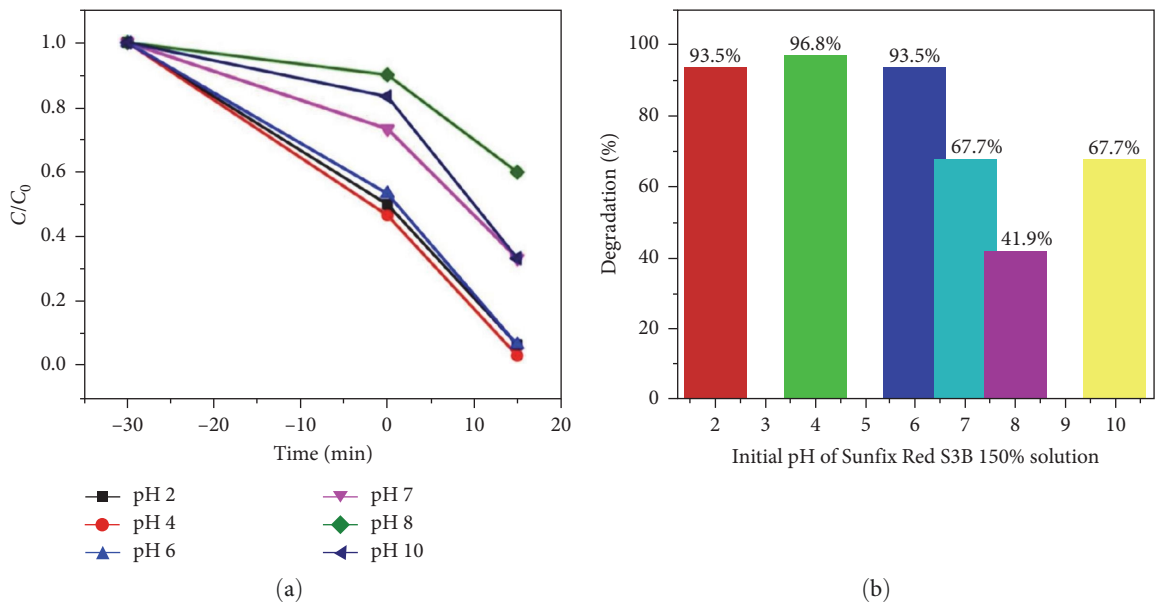

FIGURE 12: Photocatalytic behavior of HA_Ag_3PO_4(c) at different pH (a) and degradation percentage of the dye at different pH (b).

superoxide ($\cdot O_2^-$), and photogenerated holes (h^+) were trapped by IPA, ascorbic acid, and EDTA, respectively, under similar conditions. The scavengers were taken in the concentration of 1 mmol/L and the concentrations of the dye and the photocatalyst were fixed to 20 ppm and 0.5 g L^{-1}, respectively, and irradiated by direct sunlight for 60 min and the results are given in Figure 13.

From the free radicals trapping test, it can be noted that the photocatalytic degradation was decreased from 100% to 82% with the addition of IPA which reveals that role played by hydroxyl radicals in the degradation of the dye SR is only to a small extend, while the other radical trappers EDTA and ascorbic acid deteriorated the degradation of the dye significantly (46% and 35%, respectively). It is clear that the superoxide radicals and holes took part actively in the photocatalysis process.

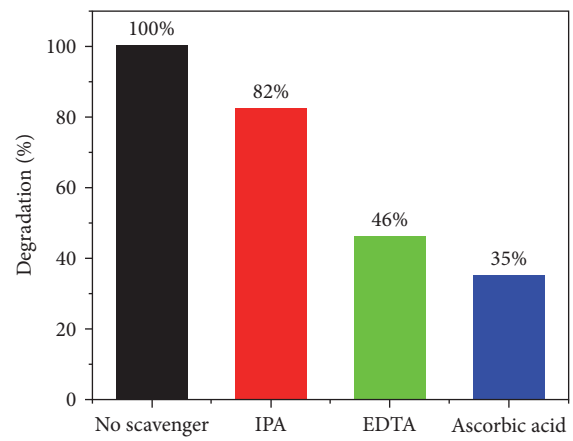

FIGURE 13: Photocatalytic behavior of HA_Ag_3PO_4(c) with scavengers.

3.2.6. Degradation of Other Dyes. The study of photocatalytic behavior of the photocatalyst HA_Ag_3PO_4(c) on some other anionic and cationic dyes was also extended. Anionic dyes such as SR S3B 150% and SB DN conc., the cationic dyes such as MB and RhB, and cocktail of all the four dyes were subjected to photodegradation by HA_Ag_3PO_4(c) under similar conditions and presented in Figure 14. The photocatalytic experiments were carried out for 150 min at 20 ppm dye concentration and photocatalyst concentration of 1 g L^{-1}. All the dyes showed different degradation rate, which is clear from Figure 14. SR and SB were decomposed completely in 30 and 60 min, respectively, while MB and RhB were decolorized to 98.16% and 78.67%, respectively, at the irradiation time 1 hr 45 min. Meanwhile, the degradation of cocktail dye solution was found to be 96.25% in 1 hr 45 min. The rate constants of the degradation of the different dyes are observed in the order $k_{SR} > k_{SB} > k_{MB} > k_{CT} > k_{RhB}$ which are depicted in Table 2.

4. Possible Photocatalytic Mechanism in the Degradation of Sunfix Red S3B 150%

From the above findings, it can be noted that the concentration of $AgNO_3$ precursor taken for the formation of HA_Ag_3PO_4 composite influenced the photocatalytic process in two ways. First, as the concentration of $AgNO_3$ increased from 0.02 to 0.08 M, it showed an increasing order of photocatalysis due to the increased number of active sites available. Meanwhile, it can be seen from the TEM results that the higher concentration of the Ag^+ precursor also resulted in reduction of particle size which led to enhanced photodegradation of dyes owing to increase in surface-to-volume ratio. In the process of photocatalytic degradation, the photogenerated electron–hole recombination inhibits the photocatalysis [27]. Hence, proper charge separation is required to make them available to carry out the redox process. Many results

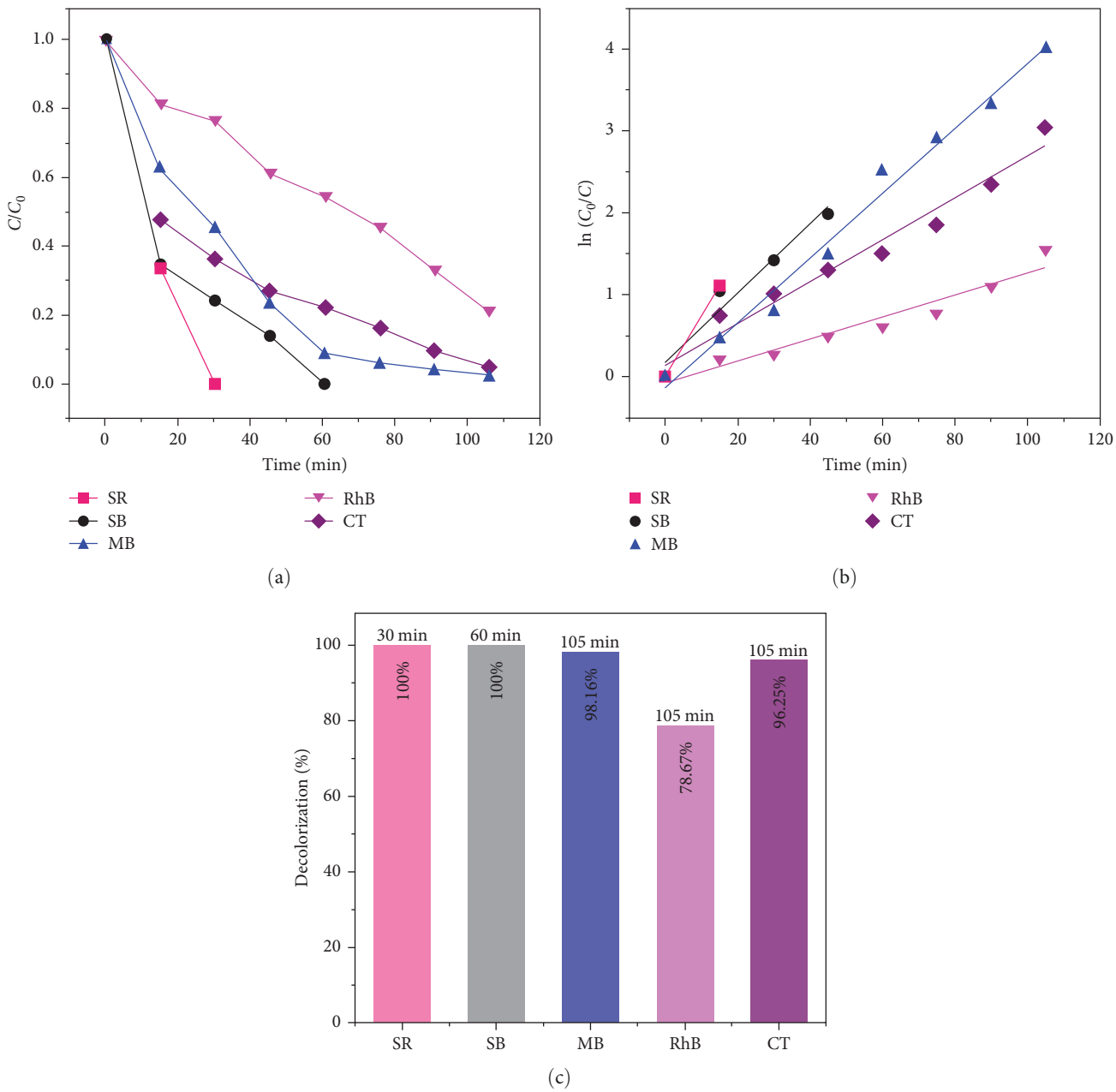

FIGURE 14: Degradation of different organic dyes by HA_Ag_3PO_4(c).

reported that heterostructures can inhibit electron–hole recombination through creating a proper transfer channel for the photogenerated charges [27, 37]. In the present work, the adopted synthesis method has resulted in good interfacial bonding between HA and Ag_3PO_4 which has been clearly noticed from the TEM result (Figure 6(f)). This channel may facilitate an easy transfer of photogenerated electrons e_{CB}^- from Ag_3PO_4 to hydroxyapatite being a good electron acceptor [38].

Based on the obtained results, the possible mechanism of photocatalytic degradation is proposed (Figure 15). In the presence of direct sunlight, the photocatalyst is excited and electron–hole pairs are generated. The majority of photogenerated holes (h_{VB}^+) in the valence band directly involve in the oxidation of the organic dye, while some of them generate some ·OH, which may contribute a weak photocatalysis, which is confirmed from the quenching test. It is also evident from the estimated value of conduction band potential (0.29 eV) of Ag_3PO_4 that it is more positive than $O_2/\cdot O_2^-$ (−0.33 eV vs. NHE) and hence the photoexcited electrons (e_{CB}^-) could not reduce the dissolved O_2 to superoxide radicals ($\cdot O_2^-$). This may result in the reduction of lattice Ag^+ to Ag metal which may eventually suppress the availability of photogenerated electrons for photocatalytic process [36]. However, hydroxyapatite in the composite captures the photogenerated electrons and makes them available for photocatalysis. Moreover, the transferred photogenerated electrons reduce the adsorbed

Table 2: Kinetic studies of HA_Ag_3PO_4(c) of the degradation of different dyes.

Dyes	Catalyst concentration ($g\,L^{-1}$)	Zero order $C_0 - C = k_0 t$		First order $\ln(C_0/C) = k_1 t$		Second order $(1/C) - (1/C_0) = k_2 t$	
		k_0 (min^{-1})	R^2	k_1 (min^{-1})	R^2	k_2 (min^{-1})	R^2
Sunfix Red (SR) S3B 150%	1	0.005	0.92857	0.07324	1	0.88889	1
Sunzol Black (SB) DN conc.	1	0.00427	0.74598	0.042	0.92443	0.45961	0.95049
Methylene blue (MB)	1	0.00989	0.821	0.03927	0.98461	0.40652	0.74271
Rhodamine B (RhB)	1	0.01059	0.98678	0.01343	0.93367	0.01983	0.77052
Cocktail (CT)	1	0.00462	0.74382	0.02544	0.96133	0.24373	0.69454

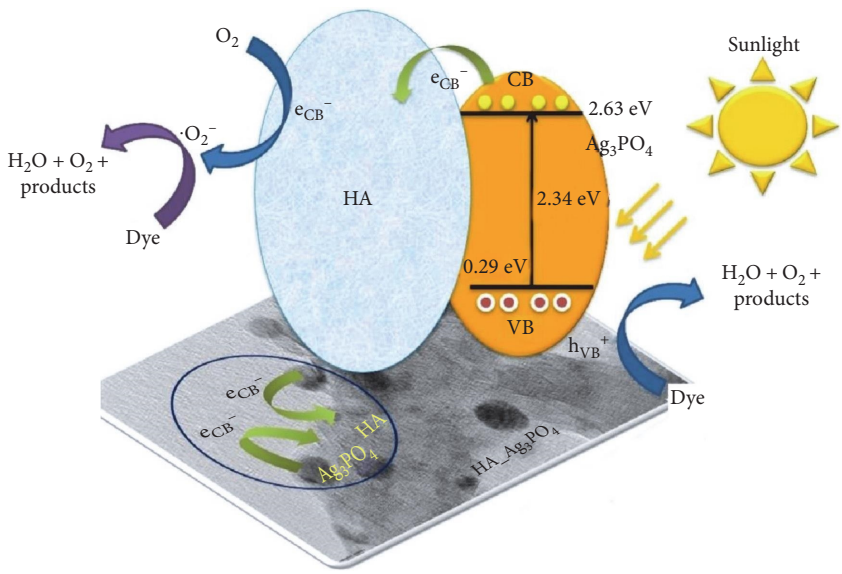

Figure 15: Possible photocatalytic mechanism.

O_2 to superoxide radicals ($\cdot O_2^-$) which actively take part in the photocatalytic degradation of the organic dye under direct sunlight.

$$HA\_Ag_3PO_4 + h\nu \longrightarrow h^+_{(VB)} + e^-_{(CB)}. \quad (8)$$

$$h^+_{(VB)} + H_2O \longrightarrow \cdot OH + H^+. \quad (9)$$

$$e^-_{(CB)} + O_2 \longrightarrow {}^{\cdot}O_2^-. \quad (10)$$

$$\text{Dye} + \cdot OH \longrightarrow \text{Degradation products}. \quad (11)$$

$$\text{Dye} + {}^{\cdot}O_2^- \longrightarrow \text{Degradation products}. \quad (12)$$

$$\text{Dye} + h^+_{(VB)} \longrightarrow \text{Degradation products}. \quad (13)$$

4.1. Reusability. The reusability of the prepared composite HA_Ag_3PO_4(c) was examined for four cycles and presented in Figure 16. The sample after every cycle of photocatalytic

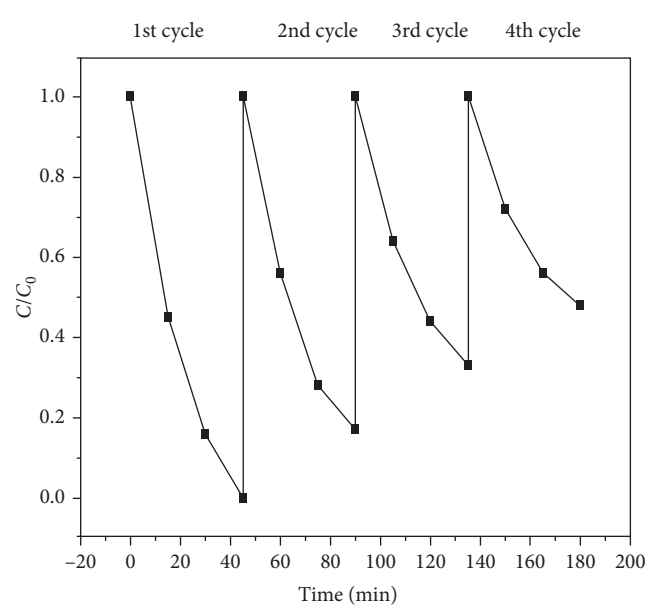

Figure 16: Recycle test of HA_Ag_3PO_4(c).

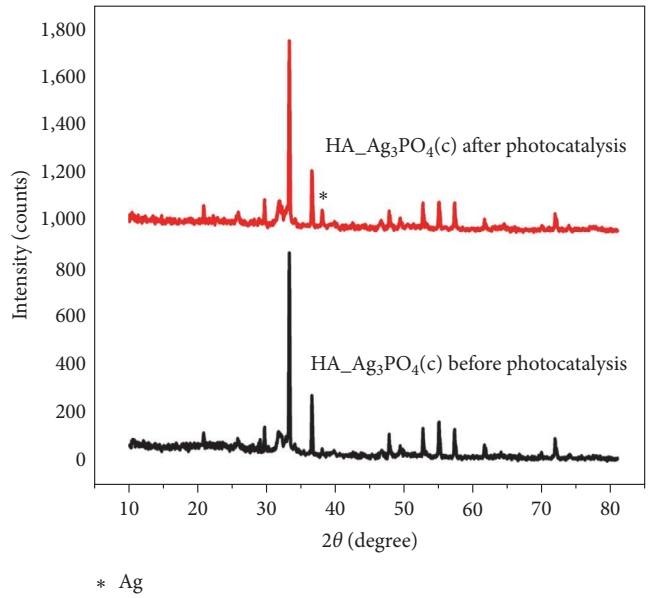

Figure 17: XRD pattern of the photocatalyst after four cycles of photodegradation.

Table 3: Comparison of removal efficiency of HA_Ag_3PO_4(c).

S. no.	Photocatalysts	Catalyst concentration ($g\,L^{-1}$)	Dyes	Dye concentration (ppm)	Time	Removal efficiency (%)	References
1	Ag_3PO_4/HAp@γ-Fe_2O_3	1.67	MB	50	4 hr	99	[39]
2	Ag_3PO_4/HAp	1	RhB	10	30 min	99	[40]
3	Ag_3PO_4/AgBr/HAp	1.4	MB	10	40 min	100	[6]
4	HA–Ag_3PO_4	0.5	SR	20	45 min	100	Present work

degradation of the dye was regenerated by washing three times with DI water and was dried at 60°C in a vacuum oven and used for the next cycle. The performance of the prepared composite declined gradually after each cycle and the degradation efficiency reduced to 52% from 100% after the fourth cycle of degradation. The photocatalyst after the fourth run was subjected to XRD analysis to investigate the stability and presented in Figure 17. The presence of the peak at 38° is corresponding to pure Ag (111) plane which reveals that the photocatalyst underwent slight photocorrosion after four cycles. The removal efficiency of the prepared sample was also compared with the previous results and presented in Table 3.

5. Conclusion

Ag_3PO_4-anchored hydroxyapatite was synthesized via a facile in situ ion-exchange method. From the results, it was found that the particle size of Ag_3PO_4 can be tuned by the concentration of $AgNO_3$ precursor solution. The photocatalytic performance on an anionic dye SR S3B 150% under visible light was carried out at different experimental conditions and found satisfactory results. The photodegradation studies were also extended for other organic dyes such as SB, MB, RhB, and cocktail of all four dyes. The studies revealed that the synthesized composites can be a proficient photocatalyst for the degradation of studied organic dyes.

Data Availability

All data generated or analyzed during this study are included in the published article.

Conflicts of Interest

The authors declare that they have no conflicts of interest.

Acknowledgments

S. Dhatchayani gratefully acknowledges UGC, New Delhi, for awarding UGC-BSR fellowship (F. No. 25-1/2014-15 (BSR)/7-14/2007(BSR)/13.03.2015) and the authors greatly acknowledge Rusa–Phase 2.0 grant sanctioned vide letter no. F. 24-51/2014-U, Policy (TNMulti-Gen), Department of Education, Government of India, Dt.09.10.2018., UGC-SAP, DST-FIST, and DST-PURSE for financial support to carry out this work. We thank Mr. N. Pandi and Mrs. P. Kanchana for the supply of dyes for the present studies and also extend our gratitude to USIC, Alagappa Uuniversity for rendering instruments for characterizations.

References

[1] A. Saravanan, P. Senthil Kumar, S. Jeevanantham et al., "Effective water/wastewater treatment methodologies for toxic pollutants removal: processes and applications towards sustainable development," *Chemosphere*, vol. 280, Article ID 130595, 2021.

[2] Y. Liu, P. Wang, B. Gojenko et al., "A review of water pollution arising from agriculture and mining activities in central Asia: facts, causes and effects," *Environmental Pollution*, vol. 291, Article ID 118209, 2021.

[3] A. Shahedi, A. K. Darban, F. Taghipour, and A. Jamshidi-Zanjani, "A review on industrial wastewater treatment via electrocoagulation processes," *Current Opinion in Electrochemistry*, vol. 22, pp. 154–169, 2020.

[4] I. H. Ali, M. K. Al Mesfer, M. I. Khan, M. Danish, and M. M. Alghamdi, "Exploring adsorption process of lead (II) and chromium (VI) ions from aqueous solutions on acid activated carbon prepared from *Juniperus procera* leaves," *Processes*, vol. 7, no. 4, Article ID 217, 2019.

[5] C. Amor, L. Marchão, M. S. Lucas, and J. A. Peres, "Application of advanced oxidation processes for the treatment of recalcitrant agro-industrial wastewater: a review," *Water*, vol. 11, no. 2, Article ID 205, 2019.

[6] N. M. Mahmoodi and M. H. Saffar-Dastgerdi, "Clean laccase immobilized nanobiocatalysts (graphene oxide-zeolite nanocomposites): from production to detailed biocatalytic degradation of organic pollutant," *Applied Catalysis B: Environmental*, vol. 268, Article ID 118443, 2020.

[7] N. M. Mahmoodi, B. Hayati, and M. Arami, "Textile dye removal from single and ternary systems using date stones: kinetic, isotherm, and thermodynamic studies," *Journal of Chemical and Engineering Data*, vol. 55, no. 11, pp. 4638–4649, 2010.

[8] N. Nasrollahi, S. Aber, V. Vatanpour, and N. M. Mahmoodi, "The effect of amine functionalization of CuO and ZnO nanoparticles used as additives on the morphology and the permeation properties of polyethersulfone ultrafiltration nanocomposite membranes," *Composites Part B: Engineering*, vol. 154, pp. 388–409, 2018.

[9] S. Sha, L. Zhang, H. Liu et al., "Synthesis and visible-light photocatalytic degradation of Ag_3PO_4/AgBr/hydroxyapatite ternary nanocomposites prepared from oyster shells," *RSC Advances*, vol. 11, no. 26, pp. 15598–15607, 2021.

[10] M. Hadei, A. Mesdaghinia, R. Nabizadeh, A. H. Mahvi, S. Rabbani, and K. Naddafi, "A comprehensive systematic review of photocatalytic degradation of pesticides using nano TiO_2," *Environmental Science and Pollution Research*, vol. 28, pp. 13055–13071, 2021.

[11] N. M. Mahmoodi, B. Hayati, M. Arami, and F. Mazaheri, "Single and binary system dye removal from colored textile wastewater by a dendrimer as a polymeric nanoarchitecture: equilibrium and kinetics," *Journal of Chemical and Engineering Data*, vol. 55, no. 11, pp. 4660–4668, 2010.

[12] X. Zhu, Y. Shi, Q. Luo et al., "High-efficiency visible-light-driven Ag_3PO_4 photocatalysts modified by conjugated polyvinyl alcohol derivatives," *Materials Research Express*, vol. 6, no. 12, Article ID 125558, 2019.

[13] P. Huang and J. Luan, "Preparation and characterization of an Ag_3PO_4/GaOOH composite with enhanced photocatalytic performance toward rhodamine B," *New Journal of Chemistry*, vol. 44, no. 6, pp. 2414–2422, 2020.

[14] N. Tavker, U. K. Gaur, and M. Sharma, "Agro-waste extracted cellulose supported silver phosphate nanostructures as a green photocatalyst for improved photodegradation of RhB dye and industrial fertilizer effluents," *Nanoscale Advances*, vol. 2, no. 7, pp. 2870–2884, 2020.

[15] M. Du, J. Chen, K. Liu, H. Xing, and C. Song, "Recent advances in biomedical engineering of nano-hydroxyapatite including dentistry, cancer treatment and bone repair," *Composites Part B: Engineering*, vol. 215, Article ID 108790, 2021.

[16] G. Wang, G. Qian, J. Zan et al., "A co-dispersion nanosystem of graphene oxide @silicon-doped hydroxyapatite to improve scaffold properties," *Materials & Design*, vol. 199, Article ID 109399, 2021.

[17] N. M. Basfer, S. F. Mansour, and M. K. Ahmed, "Physicochemical properties of hydroxyapatite modified with vanadium ions for degradation of methylene blue," *Journal of Molecular Structure*, vol. 1240, Article ID 130562, 2021.

[18] S. Dhatchayani, S. Vijayakumar, N. Sarala, B. Vaseeharan, and K. Sankaranarayanan, "Effect of curcumin sorbed selenite substituted hydroxyapatite on osteosarcoma cells: an *in vitro* study," *Journal of Drug Delivery Science and Technology*, vol. 60, Article ID 101963, 2020.

[19] A. Rout and S. Agrawal, "Structural, morphological and electrical properties of new type Dy doped $Ca_{6-x}Na_2Y_2$ $(SiO_4)_6$ $(OH)_2$ hydroxyapatite compound synthesized by co-precipitation method," *Journal of Electroceramics*, vol. 48, pp. 74–94, 2022.

[20] H. Bouyarmane, C. El Bekkali, J. Labrag et al., "Photocatalytic degradation of emerging antibiotic pollutants in waters by TiO_2/Hydroxyapatite nanocomposite materials," *Surfaces and Interfaces*, vol. 24, Article ID 101155, 2021.

[21] G. Chen, X. Zheng, C. Wang et al., "A postsynthetic ion exchange method for tunable doping of hydroxyapatite nanocrystals," *RSC Advances*, vol. 7, no. 89, pp. 56537–56542, 2017.

[22] V. Uskoković, M. A. Iyer, and V. M. Wu, "One ion to rule them all: the combined antibacterial, osteoinductive and anticancer properties of selenite-incorporated hydroxyapatite," *Journal of Materials Chemistry B*, vol. 5, no. 7, pp. 1430–1445, 2017.

[23] A. Aziz, N. Ali, A. Khan et al., "Chitosan-zinc sulfide nanoparticles, characterization and their photocatalytic degradation efficiency for azo dyes," *International Journal of Biological Macromolecules*, vol. 153, pp. 502–512, 2020.

[24] M. Manoj, D. Mangalaraj, N. Ponpandian, and C. Viswanathan, "Core–shell hydroxyapatite/Mg nanostructures: surfactant free facile synthesis, characterization and their *in vitro* cell viability studies against leukaemia cancer cells (K562)," *RSC Advances*, vol. 5, no. 60, pp. 48705–48711, 2015.

[25] Y.-G. Zhang, Y.-J. Zhu, and F. Chen, "Novel interconnected nanochannel hydroxyapatite ceramics: synthesis, microstructure, and permeability," *Ceramics International*, vol. 43, no. 7, pp. 5403–5411, 2017.

[26] R. K. Santos, T. A. Martins, G. N. Silva et al., "Ag_3PO_4/NiO composites with enhanced photocatalytic activity under visible light," *ACS Omega*, vol. 5, no. 34, pp. 21651–21661, 2020.

[27] Q. Chang, X. Meng, S. L. Hu, F. Zang, and J. L. Yang, "Hydroxyapatite/N-doped carbon dots/Ag_3PO_4 composite for improved visible-light photocatalytic performance," *RSC Advances*, vol. 7, no. 48, pp. 30191–30198, 2017.

[28] A. N. Martín-Gómez, J. A. Navío, C. Jaramillo-Páez, P. Sánchez-Cid, and M. C. Hidalgo, "Hybrid ZnO/Ag_3PO_4 photocatalysts, with low and high phosphate molar percentages," *Journal of Photochemistry and Photobiology A: Chemistry*, vol. 388, Article ID 112196, 2020.

[29] G. Bharath, B. Swarna Latha, E. H. Alsharaeh, P. Prakash, and N. Ponpandian, "Enhanced hydroxyapatite nanorods

formation on graphene oxide nanocomposite as a potential candidate for protein adsorption, pH controlled release and an effective drug delivery platform for cancer therapy," *Analytical Methods*, vol. 9, no. 2, pp. 240–252, 2017.

[30] C. C. Negrila, M. V. Predoi, S. L. Iconaru, and D. Predoi, "Development of zinc-doped hydroxyapatite by sol–gel method for medical applications," *Molecules*, vol. 23, no. 11, Article ID 2986, 2018.

[31] A. Khan, S. J. Shah, K. Mehmood, Awais, N. Ali, and H. Khan, "Synthesis of potent chitosan beads a suitable alternative for textile dye reduction in sunlight," *Journal of Materials Science: Materials in Electronics*, vol. 30, pp. 406–414, 2019.

[32] A. Dargahi, M. R. Samarghandi, Y. Vaziri, G. Ahmadidoost, E. Ghahramani, and A. A. Shekarchi, "Kinetic study of the photocatalytic degradation of the acid blue 113 dye in aqueous solutions using zinc oxide nanoparticles immobilized on synthetic activated carbon," *Journal of Advances in Environmental Health Research*, vol. 7, no. 2, pp. 75–85, 2019.

[33] M. F. Hanafi and N. Sapawe, "A review on the water problem associate with organic pollutants derived from phenol, methyl orange, and remazol brilliant blue dyes," *Materials Today: Proceedings*, vol. 31, Part 1, pp. A141–A150, 2020.

[34] K. M. Reza, A. S. W. Kurny, and F. Gulshan, "Parameters affecting the photocatalytic degradation of dyes using TiO_2: a review," *Applied Water Science*, vol. 7, pp. 1569–1578, 2017.

[35] P. Amornpitoksu, S. Suwanboon, and C. Randorn, "Photocatalytic dye decolorization under light-emitting-diode irradiation by silver halides prepared from hydrohalic acids," *Materials Research Express*, vol. 6, no. 11, Article ID 115524, 2019.

[36] R. Li, X. Song, Y. Huang, Y. Fang, M. Jia, and W. Ma, "Visible-light photocatalytic degradation of azo dyes in water by Ag_3PO_4: an unusual dependency between adsorption and the degradation rate on pH value," *Journal of Molecular Catalysis A: Chemical*, vol. 421, pp. 57–65, 2016.

[37] C. Su, L. Liu, M. Zhang, Y. Zhang, and C. Shao, "Fabrication of Ag/TiO_2 nanoheterostructures with visible light photocatalytic function *via* a solvothermal approach," *CrystEngComm*, vol. 14, no. 11, pp. 3989–3999, 2012.

[38] L.-L. Zhang, Q. Tong, X.-Y. Zhang et al., "Preparation and photocatalytic property of alumina doped zinc oxide nanoparticles supported on hydroxyapatite," *Materials Technology*, vol. 29, no. sup2, pp. A9–A13, 2014.

[39] X. N. Pham, H.-T. Le, T.-T. Nguyen, and N.-T. Pham, "Ag_3PO_4-supported magnetic hydroxyapatite composite as green photocatalyst for the removal of cationic and anionic dyes from aqueous solution," *Chemical Engineering & Technology*, vol. 44, no. 10, pp. 1850–1862, 2021.

[40] U. Sulaeman, S. Suhendar, H. Diastuti, A. Riapanitra, and S. Yin, "Design of Ag_3PO_4 for highly enhanced photocatalyst using hydroxyapatite as a source of phosphate ion," *Solid State Sciences*, vol. 86, pp. 1–5, 2018.